Tailoring the electronic structure of half-metallic Heusler alloys

P. Klaer,[1] M. Kallmayer,[1] C. G. F. Blum,[2] T. Graf,[2] J. Barth,[2] B. Balke,[2] G. H. Fecher,[2] C. Felser,[2] and H. J. Elmers[1,*]
[1]*Institut für Physik, Johannes Gutenberg–Universität Mainz, D-55099 Mainz, Germany*
[2]*Institut für Anorganische Chemie und Analytische Chemie, Johannes Gutenberg–Universität Mainz, D-55099 Mainz, Germany*
(Received 29 July 2009; revised manuscript received 4 September 2009; published 9 October 2009)

We investigated element-specific magnetic moments and the spin-resolved unoccupied density of states (DOS) of polycrystalline Co_2TiZ (Z=Si, Ge, Sn, Sb), $Co_2Mn_xTi_{1-x}Si$ and $Co_2MnGa_{1-x}Ge_x$ Heusler alloys using circular dichroism in x-ray absorption spectroscopy (XMCD). We find a small ($<0.03\mu_B$) Ti moment oriented antiparallel and a large ($>3\mu_B$) Mn moment oriented parallel to the Co moment of approximately $1\mu_B$ per atom in the investigated compounds. Orbital magnetic moments are increased for quaternary compounds compared to the corresponding ternary compounds with $x=0$ or $x=1$. The unoccupied spin-resolved partial DOS at the Co atom was extracted from the XMCD data. In the case of Co_2TiSi, Co_2TiGe, and Co_2TiSn, the Co minority DOS reveals a maximum at 0.5 eV above E_F and very low values at E_F in agreement with the expectation for half-metallic ferromagnetism. In contrast, Co_2TiSb shows a large minority DOS at the Fermi energy like a normal metal. A substitution of Ti by Mn in Co_2TiSi shifts the minority DOS maximum from 0.5 to 0.9 eV with respect to the Fermi energy. For the series $Co_2MnGa_{1-x}Ge_x$ we observe a gradual shift of the minority DOS maximum from 0.7 eV for $x=1$ to 1.0 eV for $x=0$, indicating half-metallic ferromagnetism for the whole series. Our results, revealing the distribution of magnetic moments and the relative position of the Fermi energy as a function of the number of valence electrons, confirm the predicted possibility of tailoring the minority band gap using substitutional quaternary Heusler compounds. The results maybe of general importance for the understanding of the electronic structures in complex intermetallic compounds.

DOI: 10.1103/PhysRevB.80.144405 PACS number(s): 71.20.−b, 75.47.−m, 75.50.Cc, 78.70.Dm

I. INTRODUCTION

Half-metallic ferromagnetism (HMF) (Refs. 1 and 2) has become a vivid research topic. Half-metallic ferromagnets have only one spin channel for conduction at the Fermi level, where the other channel has a band gap across the Fermi level.[1] This property turns HMF materials into very attractive materials for the fabrication of spintronic devices.[3–7] Co-based Heusler alloys Co_2YZ (transition metal Y and main group element Z) are particularly interesting because *ab initio* theory has predicted HMF and a high Curie temperature for many of these compounds.[1,8–10]

Recent experimental progress in the fabrication of tunneling magnetoresistance (TMR) devices provides indirect evidence for HMF in Heusler alloys. The first TMR devices with $Co_2(Cr_{0.6}Fe_{0.4})Al$ as electrode material showed moderate TMR values of 16% at room temperature.[3] Recently, considerably larger TMR values have been reported for TMR devices using Co_2MnSi (Refs. 4, 5, and 7) and $Co_2Fe(Al_{0.5}Si_{0.5})$ (Ref. 11) electrodes. The strong temperature dependence of the TMR effect was attributed to the location of the Fermi energy close to one of the minority band edges.[12] In order to shift the Fermi energy into the center of the band gap, a band-structure tailoring through substitution of the transition metal on the Y site or the main group element on the Z site in quaternary compounds has been proposed.[6,10,12–14] An example is $Co_2Fe(Al_{0.5}Si_{0.5})$ (Ref. 6) for which *ab initio* calculations predict the Fermi energy E_F to be in the center of the minority gap in contrast to Co_2FeAl and Co_2FeSi, where E_F is close to the upper or lower edge of the gap.[15,16] Shan *et al.*[17] recently presented a tunneling spectroscopy study that supports the position of E_F in the gap center for $Co_2Fe(Al_{0.5}Si_{0.5})$. A similar shift has been proposed for $Co_2(Fe_xMn_{1-x})Si$ (Ref. 18) and tested by photoemission spectroscopy without spin resolution.[19,20]

A direct study of the band gap is of particular importance to confirm the theoretical concept of a gradual band-structure tailoring. We apply x-ray magnetic circular dichroism (XMCD) in photoabsorption spectroscopy (XAS) to study the element-specific electronic structure, both at surfaces and at buried interfaces.[21]

In principle, the L edge absorption spectra for left and right circular polarized x-ray lights reflect the spin-resolved partial density of states (PDOS) at $3d$ transition-metal atoms.[22,23] However, for strongly localized states, e.g., in an oxide, the strong interaction of the core hole with the conduction band in the final state leads to an additional splitting of the spectra, often denoted as multiplet effects.[24] These multiplet effects may effectively mask the band structure, and in this case it is impossible to disentangle PDOS and multiplet contributions. Telling *et al.*[25] pointed out the existence of strongly localized moments at the Y site in Heusler compounds. These localized moments give rise to a pronounced multiplet structure in the absorption spectra. In contrast, previous results of the Co and Ni L edge in intermetallic compounds clearly revealed PDOS related features in the absorption spectra of Heusler alloys.[26,27]

Electronic states related to the Co atoms are of particular importance for the HMF properties in Heusler compounds. Theoretical results relate the origin of the minority band gap in Heusler compounds[8,28,29] to the hybridization of Co and Y $3d$ orbitals, whereas the width of the gap is determined by the Co-Co hybridized states. The latter states exhibit a crystal-field splitting of the Co $3d$ states into antibonding occupied t_{2g} (t_{1u}) and unoccupied e_g (e_u) states that are closest to the Fermi energy.[28] Recently, we have shown that the Co PDOS can be recovered from XAS/XMCD data[30] by a

proper consideration of the final-state effects. For epitaxial $Co_2(Fe_xMn_{1-x})Si$ and $Co_2Fe(Al_{1-x}Si_x)$ films grown on MgO(100), a variation in the position of E_F within the minority band gap with the substitution could be confirmed.

In this paper, we focus on polycrystalline samples of the substitutional variations of Co_2TiZ (Z=Si, Ge, Sn, Sb), $Co_2Mn_xTi_{1-x}Si$, and $Co_2MnGa_{1-x}Ge_x$ Heusler alloys. All compounds with $x=0$ or $x=1$ (except Co_2TiSb) have been predicted to be half-metallic ferromagnets.[31] Experiments revealed magnetization values following the generalized Slater-Pauling rule.[32,33] This rule relates the magnetization to the number of valence electrons N_v per formula unit according to $\mu/\mu_B=N_v-24$. Co_2TiZ (Z=Si, Ge, Sn) are interesting Heusler alloys because the half-metallic properties of Co_2TiZ are less sensitive to local atomic disorder in contrast to many other Heusler alloys.[32] As a counterexample, we investigate Co_2TiSb. The exchange of the fourth main group element by the fifth group element results in normal-metallic ferromagnetic properties.[31] Substitution of Ti by Mn in Co_2TiSi implies the prospect of combining the robust half-metallic properties of Co_2MnSi with the disorder-resistant properties of Co_2TiSi. The idea of substituting the main group element in order to shift the Fermi energy relative to the band gap as proposed for $Co_2Fe(Al_{1-x}Si_x)$ (Refs. 15 and 34) is studied by the $Co_2MnGa_{1-x}Ge_x$ series.

We determine changes of the element-specific spin and orbital moments of the Co and Y elements with composition and compare the results with theoretical predictions. We are, in particular, interested in the contributions of the orbital magnetic moment as those reveal contributions from spin-orbit coupling.[35] Fine structures of the Co $L_{2,3}$ edge spectra are tested against an interpretation as multiplet effects by comparison with multiplet calculations including charge transfer and Slater integral reduction. We then extract the Co PDOS for all samples following the method described in Ref. 30. For the compounds with $x=0$ and $x=1$, the Co PDOS is in good agreement with theoretical predictions. The anticipated shift of the Fermi energy with respect to the minority band gap in half-metallic compounds is confirmed for the case of $Co_2MnGa_{1-x}Ge_x$.

II. EXPERIMENTAL

The polycrystalline samples were prepared by arc melting of stoichiometric quantities of the constituents in an argon atmosphere (10^{-4} mbar). Care was taken to avoid oxygen contamination. This was established by evaporation of Ti inside of the vacuum chamber before melting the compound as well as additional purification of the process gas. The melting procedure was repeated three times to get a homogeneous material. After melting, the polycrystalline ingots were annealed in an evacuated quartz tube at 1073 K for 8 days. For powder investigations, a part of the sample was crushed by hand using a mortar. The structure was investigated by x-ray diffraction (XRD) using excitation by Mo K_α (Bruker, D8) radiation of powder samples. The magnetic properties were investigated by a superconducting quantum interference device [(SQUID) Quantum Design MPMS-XL-5)] using nearly punctual pieces of approximately 10–20 mg of the sample. Rods with dimensions $1\times1\times10$ mm^3 were cut from the ingots for spectroscopic investigations of the bulk samples.

The XAS experiments were performed at the UE56/1-SGM beamline at the German synchrotron light source BESSY II. The samples were fractured *in situ* in UHV ($p=1\times10^{-9}$ Torr) directly before the measurement. An Au mesh monitored the incident photon flux. The total electron yield (TEY) served as a measure for the x-ray absorption signal. The sample was shielded by a conducting tube in order to collect all electrons. An external magnetic field of 1.22 T was applied along the direction of the incident x-ray beam, i.e., approximately perpendicular to the sample surface, and switched after each data point to determine the XMCD signal while the polarization was kept constant (see details in Ref. 36). The energy resolution of the x-ray monochromator was set to approximately 0.4 eV at 800 eV. An increase in the resolution to 0.1 eV at 800 eV for selected samples revealed only marginal changes of the observed spectra. This confirmed that the spectral shape is dominated by the intrinsic lifetime broadening of x-ray absorption.

After the measurements, we verified the composition and the homogeneity of the fractured surfaces of all samples using energy dispersive x-ray (EDX) fluorescence in a scanning electron microscope. One should note that the accuracy of the determination of the relative atomic concentration with EDX is on the order of ±2 at. %, only.

III. MAGNETIC PROPERTIES OF Co_2TiZ

The EDX analysis of the fractured surfaces revealed a homogeneous composition for all samples with small deviations from the stoichiometric composition. We obtained relative atomic compositions for the elements Co, Ti, and Z of (49%, 23%, 28%) for Z=Si, (50%, 23%, 27%) for Z=Ge, (53%, 25%, 22%) for Z=Sn, and (49%, 26%, 25%) for Z=Sb. X-ray diffraction revealed a diffraction pattern that is compatible with a high degree of $L2_1$ order (see Ref. 37 for details). The Curie temperature T_C is 380 K for Z=Si and 355 K for Z=Ge, Sn. For Z=Sb, the magnetization showed only a small magnetization decrease in the temperature range below 400 K, indicating a much higher value of T_C. The low-temperature (5 K) magnetization is $1.96\mu_B$, $1.94\mu_B$, $1.97\mu_B$, and $1.67\mu_B$ for Z=Si, Ge, Sn, and Sb, respectively. This is in good agreement with the Slater-Pauling rule for Z=Si, Ge, and Sn.[33]

Figure 1 shows XAS/XMCD spectra at the Co and Ti $L_{2,3}$ absorption edges measured at room temperature. After subtracting a constant background from the raw data, the XAS spectra were normalized at the postedge value. The spectra for Z=Si, Ge, and Sn show similar features. The Co XAS signal reveals a characteristic double peak feature at the L_3 edge and a shoulder at the L_2 edge. An additional peak is visible at the L_3 maximum of the XMCD signal. For the case of Z=Sb, the double peak feature is completely absent. The extra peak at approximately 4 eV above the Co XAS maximum, that is, regularly observed for the Co_2YZ Heusler compounds,[38] appears only as a weak shoulder for Heusler compounds with Y=Ti.

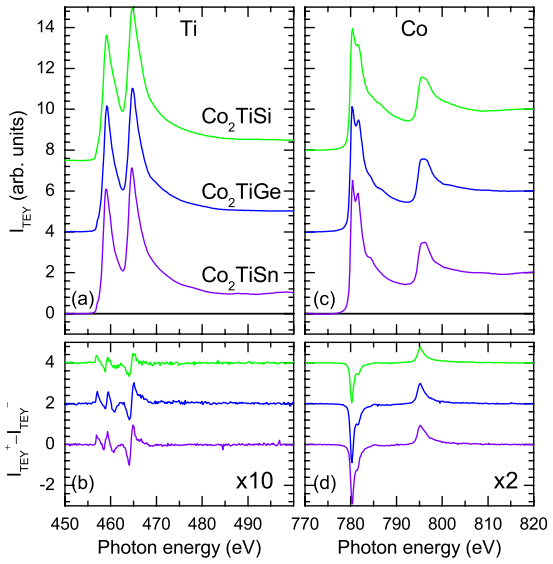

FIG. 1. (Color online) (a) X-ray absorption spectra of Co_2TiZ (Z= Si, Ge, and Sn) measured at 300 K at the Ti $L_{2,3}$ edge averaged from parallel (antiparallel) magnetization direction $I^{+(-)}_{TEY}$. (b) Corresponding XMCD spectra $I^{+}_{TEY}-I^{-}_{TEY}$ shown on the same scale (note the scaling factor of 10). (c) and (d) Similar data measured at the Co $L_{2,3}$ edge.

The Ti XAS signal shows a larger maximum at the L_2 edge compared to the L_3 edge, thus, reversing the branching ratio expected from an atomic model. This is in agreement with previously measured XAS spectra of metallic Ti.[39] The Ti shape of the XAS signal is similar to the pure element spectrum. In contrast, Ti oxide is known to reveal additional multiplet peaks. Their absence confirms the presence of a clean surface. After several hours at $p=10^{-9}$ mbar, we observed the onset of oxide derived XAS peaks. The Ti XMCD signal reveals a complex behavior of alternating positive and negative values for Z=Si, Ge, and Sn. This feature is similar to a reference XMCD spectrum measured for an ultrathin Ti film that was polarized between two ferromagnetic films.[39] From a comparison with this reference spectrum, we conclude that the Ti magnetic moment is antiparallel to the Co moment. Therefore, Co_2TiZ (Z=Si, Ge, and Sn) are ferrimagnetic compounds. For Z=Sb, the Ti XMCD signal vanishes within error limits (see Fig. 2).

Spin and orbital moments that were calculated using the sum rules are summarized in Table I. We have assumed N_h(Co)=2.5 and N_h(Ti)=8 for the number of $3d$ holes. We neglected the dipole term for the calculation of the spin moment. This contribution cancels for the polycrystalline samples investigated here.[40] We also dispensed with the self-absorption correction[41] because this correction is smaller than the statistical error for the compounds investigated here. For Co_2TiGe and Co_2TiSn, the sum-rule analysis led to very large values and opposite sign of the orbital moments. In these two cases, we determined the magnetic moment of Ti by a comparison of XMCD peak heights with data from Z =Si. The sum of the atomic moments μ_{XMCD} agrees well with the magnetization determined by SQUID magnetometry except for the case of Z=Si. In this case, XMCD leads to a slightly smaller value, which might be explained by a non-

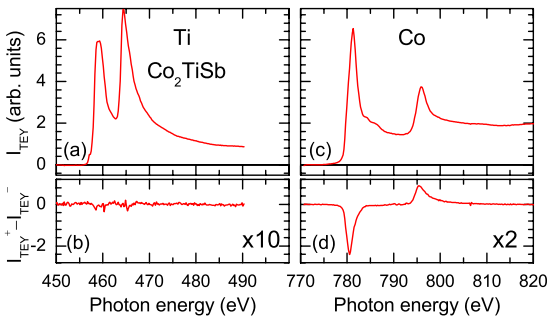

FIG. 2. (Color online) (a) X-ray absorption spectra of Co_2TiSb measured at 300 K at the Ti $L_{2,3}$ edge averaged from TEY intensities for magnetization direction parallel (antiparallel) to the x-ray polarization $I^{+(-)}_{TEY}$. (b) Corresponding XMCD spectra $I^{+}_{TEY}-I^{-}_{TEY}$ shown on the same scale (note the scaling factor of 10). (c) and (d) Similar data measured at the Co $L_{2,3}$ edge.

saturated magnetization due to the limitation of the external field for the XMCD measurement. For all Co_2TiZ compounds, the magnetization is clearly dominated by the Co spin moment and a relatively large contribution of the Co orbital moment (see Table I).

The Co XAS spectrum of Co_2TiSn measured by Yamasaki *et al.* (Ref. 42) differs from the spectra observed here. It revealed three peaks with a separation of 0.5 eV at the L_3 edge instead of two peaks. This feature was then interpreted as a multiplet effect. However, as shown in Sec. VI, the

TABLE I. Comparison of element-specific magnetic moments derived from sum-rule analysis and SQUID magnetometry for Co_2TiZ (Z=Si, Ge, Sn, and Sb for T=300 K. The sum moment μ_{XMCD} results from a weighted sum of the atomic moments. Values are given in μ_B per atom for element-specific moments and μ_B per formula unit for the magnetization. For the number of unoccupied $3d$ states, we assumed the values N_h(Co)=2.5 and N_h(Ti)=8. The error bar for the XMCD derived values does not include systematic errors due to background subtraction, saturation correction, and the error of N_h.

	μ	Co	Ti	μ_{Co}/μ_{Ti}
Z=Si	μ_{spin}	0.36±0.02	−0.02±0.02	−36
	μ_{orb}	0.02±0.02	0.00±0.02	
	μ_{XMCD}	0.75±0.12		
	μ_{SQUID}	1.21±0.10		
Z=Ge	μ_{spin}	0.49±0.02	−0.03±0.02	−33
	μ_{orb}	0.07±0.02	0.00±0.02	
	μ_{XMCD}	1.09±0.12		
	μ_{SQUID}	1.22±0.10		
Z=Sn	μ_{spin}	0.56±0.02	−0.03±0.02	−37
	μ_{orb}	0.05±0.02	0.00±0.02	
	μ_{XMCD}	1.19±0.12		
	μ_{SQUID}	1.28±0.10		
Z=Sb	μ_{spin}	0.67±0.02	0.00±0.02	
	μ_{orb}	0.05±0.02	0.00±0.02	
	μ_{XMCD}	1.44±0.12		
	μ_{SQUID}	1.62±0.10		

TABLE II. Relative concentration given as percentages of the samples from the $Co_2(Mn_xTi_{1-x})Si$ series according to an EDX analysis. The error is approximately 2%.

x	Co	Mn	Ti	Si
0.0	49.0	0.0	23.0	28.0
0.4	51.6	10.0	14.3	24.1
0.6	48.9	14.9	8.7	27.5
0.8	43.9	18.5	9.5	28.1
1.0	47.9	25.3	0.0	26.8

multiplet calculation neither reproduces the experimentally observed XAS and XMCD spectra of Ref. 42 nor the spectra observed here. XAS/XMCD spectra calculated by Bekenov *et al.* (Ref. 43), using an *ab initio* local-density approximation (LDA) approach, revealed a sharp maximum at the L_3 edge followed by a distinct shoulder at the trailing edge 1 eV above the maximum. This is in fair agreement with the spectra observed in this work. According to the band-structure calculations, the double peak at the L_3 edge observed for Z =Si, Ge, and Sn originates from a twin peak of the minority PDOS 0.5 eV above E_F with the peak at higher energy attributed to a localized Co-Ti hybridization state. Co_2TiSb has a different band structure. Due to the increased number of valence electrons, the minority band gap is shifted below E_F and a PDOS minority maximum coincides with E_F.[31] Thus, the pronounced differences between Z=Si, Ge, Sn, and Z =Sb can be traced back to the PDOS.

IV. MAGNETIC PROPERTIES OF $Co_2(Mn_xTi_{1-x})Si$

The EDX analysis resulted in some deviations from the intended composition as shown in Table II. In addition, the samples showed traces of a decomposition into a Ti-rich and a Ti-poor Heusler compound with the Co and Si concentration being constant across the fractured surface. The XRD analysis revealed a single $L2_1$ Heusler phase with a linearly varying lattice constant from 5.74 Å for x=0 to 5.65 Å for x=1.

As T_C increases from 380 K for Co_2TiSi to 985 K for Co_2MnSi, the XAS measurements were performed at 150 K, i.e., at a temperature where the thermal decrease in the magnetization is comparatively small for all compounds. Figure 3 shows XAS/XMCD spectra at the Co and Mn $L_{2,3}$ absorption edges. After subtracting a constant background from the raw data, the XAS spectra were normalized at the postedge value. The characteristic double peak features of the Co XAS and XMCD signal gradually vanish with decreasing Ti concentration. For Co_2MnSi, a very pronounced peak at 4 eV above the XAS maximum is observed in agreement with previously published spectra.[25,44] We also confirmed the fine structure of the L_3 XMCD maximum discussed in Ref. 25.

The Ti XAS/XMCD spectra (not shown here) appear similar to the spectra shown in the previous section. In particular, the sign of the Ti XMCD spectra does not change indicating the antiparallel orientation of its magnetic moment.

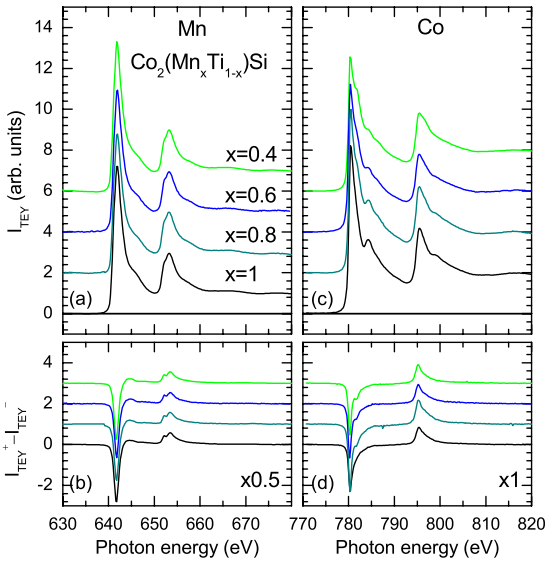

FIG. 3. (Color online) (a) X-ray absorption spectra of $Co_2(Mn_xTi_{1-x})Si$ at the Mn $L_{2,3}$ edge averaged from TEY intensities measured at 150 K for magnetization direction parallel (antiparallel) to the x-ray polarization $I^{+(-)}_{TEY}$. (b) Corresponding XMCD spectra $I^{+}_{TEY}-I^{-}_{TEY}$ shown on the same scale (note the scaling factor of 0.5). (c) and (d) Similar data measured at the Co $L_{2,3}$ edge.

The Mn XMCD signal for x=1 reveals a weak doublet structure at the Mn $2p_{1/2}$ edge. A similar splitting of the Mn L_2 XAS peak is observed for Mn oxide, however, with a larger width of the splitting and also accompanied by additional peaks at the L_3 edge.[45] Moreover, for Mn oxide, the double peak would not show up in the XMCD spectra since the Mn oxide has no magnetic moment. Other proposed explanations for the Mn multiplet features referring to interface effects[46] are not applicable in our case since we investigate an uncoated surface. Instead, the Mn L_2 double peak can be explained by a multiplet effect[47] invoked by the localized character of the Mn states.[48]

For the $Co_2(Mn_xTi_{1-x})Si$ series, the number of valence electrons N_v increases from 26 to 29. Hence, the magnetization is expected to increase linearly from $2\mu_B$/f.u. (f.u. =formula unit) to $5\mu_B$/f.u. with increasing Mn concentration. This expectation is roughly confirmed by the experiment (see Table III). The Co moment is approximately $1\mu_B$. The Mn moment is also fairly constant independent on x. Therefore, the magnetization increase with increasing x is mainly caused by the replacement of Ti with nearly zero moment by Mn with a large moment. The total magnetization for the mixed compounds is slightly larger than predicted by the Slater-Pauling rule. This was also observed in the case of a $Co_2Mn_{1-x}Fe_xAl$ series.[49] The Co orbital to spin moment ratio is larger for the mixed compounds than for x =0 and x=1. We tentatively attribute the increased orbital moment to the internal stress and local deviation of individual unit cells from their averaged cubic symmetry. The random replacement of Ti by the smaller Mn atom therefore acts as a point defect. This model is in agreement with the single phase observed in XRD because diffraction is exclusively sensitive to the translational symmetry on a much larger scale. However, a local decomposition into a few num-

TABLE III. Element-specific magnetic moments derived from sum rule for $T=150$ K analysis and SQUID magnetometry for $Co_2(Mn_xTi_{1-x})Si$ as in Table I. The sum moment μ_{XMCD} results from a weighted sum of the atomic moments. Values are given in μ_B per atom for element-specific moments and μ_B per formula unit for the magnetization. For the number of unoccupied $3d$ state, we assumed the values $N_h(Co)=2.5$, $N_h(Mn)=4.5$, and a correction factor $c_{jj}=1.4$ for Mn to account for jj mixing reduction. The Ti moment was neglected for the calculation of the sum moment as it is less than 0.02 μ_B.

	μ	Co	Mn	μ_{Co}/μ_{Mn}
$x=1$	μ_{spin}	0.72 ± 0.02	3.34 ± 0.10	0.22
	μ_{orb}	0.05 ± 0.01	0.11 ± 0.05	
	μ_{XMCD}	4.99 ± 0.20		
$x=0.8$	μ_{spin}	0.97 ± 0.02	3.39 ± 0.10	0.29
	μ_{orb}	0.09 ± 0.02	0.21 ± 0.10	
	μ_{XMCD}	5.00 ± 0.20		
$x=0.6$	μ_{spin}	0.90 ± 0.02	3.08 ± 0.10	0.30
	μ_{orb}	0.05 ± 0.02	0.12 ± 0.05	
	μ_{XMCD}	3.82 ± 0.20		
$x=0.4$	μ_{spin}	0.88 ± 0.02	3.37 ± 0.10	0.27
	μ_{orb}	0.07 ± 0.02	0.11 ± 0.05	
	μ_{XMCD}	3.29 ± 0.20		

ber of complete Co_2MnSi and Co_2TiSi unit cells cannot be fully excluded because the internal stress would in this case also destroy the local cubic symmetry and increase the orbital moment.

V. MAGNETIC PROPERTIES OF $Co_2Mn(Ga_{1-x}Ge_x)$

The EDX analysis of this series revealed a homogeneous composition for all samples except for the sample with $x=0.2$, where a small variation in the Ge/Ga ratio across the sample was observed. We obtained relative atomic compositions according to Table IV.

X-ray diffraction revealed a $L2_1$ compatible pattern for this series of samples. The almost equal scattering cross section of the constituting elements hinders an unambiguous structural determination from XRD. NMR measurements at the Mn resonance revealed a $L2_1$ structure with a small degree of disorder.[50] Because the Curie temperature T_C at approximately 900 K for the whole series is very high, the XAS/XMCD measurements were performed at room temperature. The magnetization measured by SQUID magnetometry revealed a reduction of 5% at room temperature from its low-temperature value at 5 K. The magnetization increases linearly from $4\mu_B$/f.u. to $5\mu_B$/f.u. with increasing Ge concentration in close agreement with the Slater-Pauling rule.

TABLE IV. Relative concentration given as percentages of the samples from the $Co_2Mn(Ga_{1-x}Ge_x)$ series according to an EDX analysis.

x	Co	Mn	Ga	Ge
1.0	47.9	25.3	0.0	26.8
0.8	45.7	26.1	5.7	22.5
0.6	48.0	24.8	10.9	16.3
0.4	48.5	23.9	16.9	10.7
0.2	48.6	24.3	21.8	5.3
0.0	47.7	24.7	27.6	0.0

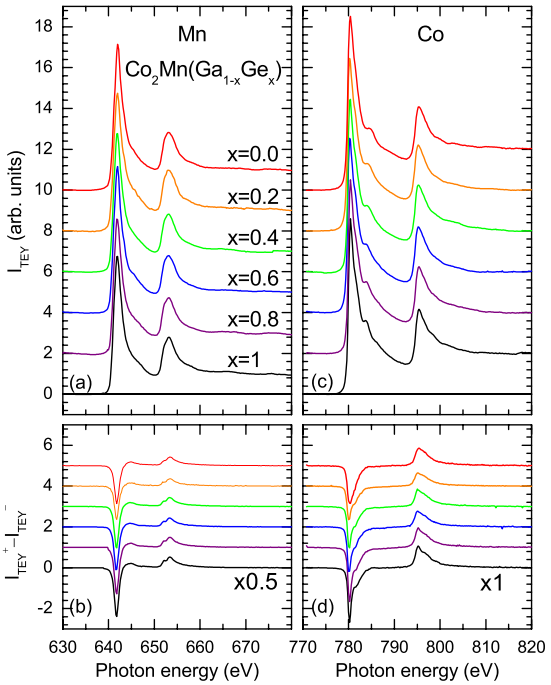

FIG. 4. (Color online) (a) X-ray absorption spectra of $Co_2Mn(Ga_{1-x}Ge_x)$ at the Mn $L_{2,3}$ edge averaged from TEY intensities measured at 300 K for magnetization direction parallel (antiparallel) to the x-ray polarization $I^{+(-)}_{TEY}$. (b) Corresponding XMCD spectra $I^{+}_{TEY}-I^{-}_{TEY}$ shown on the same scale (note the scaling factor of 0.5). (c) and (d) Similar data measured at the Co $L_{2,3}$ edge.

Figure 4 shows XAS/XMCD spectra at the Co and Mn $L_{2,3}$ absorption edges measured at room temperature. Similar to the case of $Co_2(Mn_xTi_{1-x})Si$, the Mn XMCD signal reveals a doublet feature at the Mn L_2 edge for Co_2MnGe in agreement with an earlier observation.[48] The double peak feature becomes less prominent with decreasing Ge concentration, indicating a decrease in the localization similar to the case of Co_2MnAl/Co_2MnSi discussed in Ref. 25.

The Co XAS spectra of Co_2MnGe reveal the Heusler peak at 3 eV above the L_3 maximum in accordance with the spectra reported in Ref. 48. This extra peak shifts continuously to 4 eV above the maximum with decreasing Ge concentration. One would not expect this continuous shift, if the local structure was decomposed in Ge and Ga rich areas. Therefore, the Co XAS spectra of this series unambiguously prove the formation of a Heusler structure with the Z sites randomly occupied by Ge and Ga.

The XMCD maximum at the Co L_3 edge shows a shoulder at around 1.5 eV above the maximum. A similar feature was observed in Ref. 48 and also in the case of the isoelectronic compound Co_2MnSi (Ref. 45). The shoulder has been

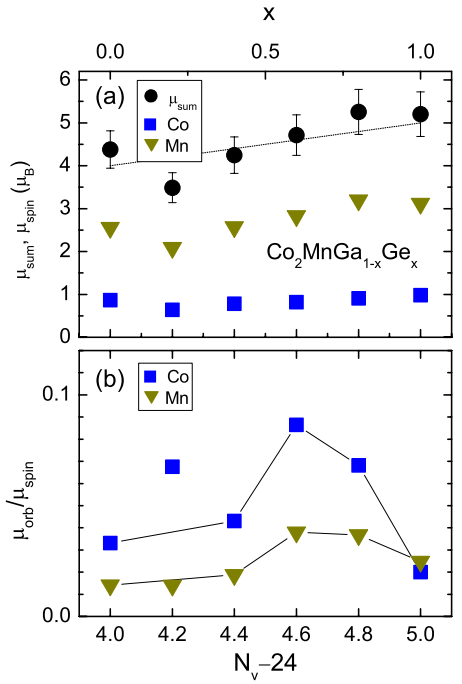

FIG. 5. (Color online) (a) Total magnetic moments (circles) and element-specific spin moments for $Co_2Mn(Ga_{1-x}Ge_x)$ measured at 300 K as a function of the Ge concentration. The solid line indicates the Slater-Pauling rule. (b) Ratio of the orbital magnetic moment over the spin magnetic moment.

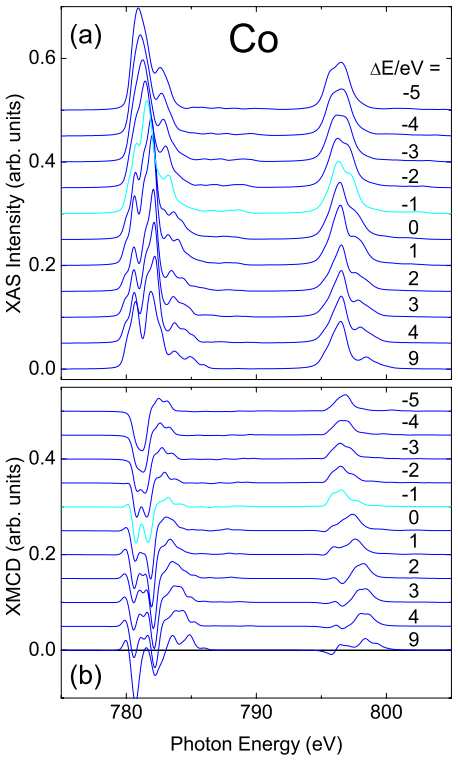

FIG. 6. (Color online) (a) Series of XAS charge-transfer multiplet calculations for the Co $2p^63d^7$ plus $2p^63d^8$ ground state for steps of 1 eV for the charge-transfer energy. The top spectrum corresponds to N_h=2.19 and the top bottom spectrum to N_h=2.94. The spectrum corresponding to the value of N_h=2.5 calculated by band-structure calculations is highlighted. (b) XMCD spectra calculated for the same parameters.

ascribed to the separated minority states with e_g and t_{2g} symmetries.[48]

The Co and Mn magnetic spin moments calculated by the sum-rule analysis increase with increasing Ge concentration as shown in Fig. 5(a). The weighted sum of Co and Mn spin and orbital moments obeys the Slater-Pauling rule. The sample with x=0.2 shows an exceptional low value, which might be traced back to the poorer homogeneity observed by the EDX analysis for this particular sample.

The orbital to spin moment ratio [Fig. 5(b)] shows a pronounced maximum between x=0.6 and x=0.8. As for the case of $Co_2(Mn_xTi_{1-x})Si$, we attribute the orbital moment increase to the internal stress and local deviation of individual unit cells from their averaged cubic symmetry. Because a local decomposition can be excluded for the $Co_2Mn(Ga_{1-x}Ge_x)$ series, the Ga atoms act as point defects in the Co_2MnGe structure. The particularly low values of the orbital moments in the case of x=1 ($0.02\mu_B$) and x=0 ($0.03\mu_B$) are in very good agreement with theoretical predictions [$0.02\mu_B$ for x=1 (Ref. 9) and $0.01-0.02\mu_B$ for x=0 (Ref. 51)].

VI. ELECTRON CORRELATION IN X-RAY ABSORPTION

In the proper description of x-ray absorption, the atom is excited from an initial-state configuration to a final-state configuration, e.g., $2p^63d^7$ to $2p^53d^8$. When open shells with more than one state need to be considered, correlation effects between the electrons lead to multiplet effects.[24]

Previous results on x-ray absorption spectroscopy have shown that the existence of local moments gives rise to pronounced multiplet structures resulting from the interaction of the core hole with the excited electron, thus, representing a final-state effect.[25,47,52,53] The consideration of final-state effects exceeds state-of-the-art band-structure calculation schemes. Nevertheless, multiplet features might be accurately described by an atomic model in the case of localized electronic states as they are discussed for Heusler alloys. We focus here on the discussion of Co states with 3d character as these states are closest to the Fermi energy. We present multiplet calculation based on the program described in Refs. 24, 54, and 55 in Fig. 6. The charge-transfer multiplet calculation considers electric dipole allowed transitions between a mixed Co $2p^63d^7$ and $2p^63d^8$ ground state and the corresponding final states $2p^53d^8$ and $2p^53d^9$. The crystal field was set to zero. The calculated results were convoluted by a Lorentzian of Γ=0.1 (0.3) eV for the L_3 (L_2) edge to account for intrinsic lifetime broadening and a Gaussian of σ=0.2 eV for the instrumental broadening according to previously published calculations.[24] Note that the realistic lifetime broadening is larger. The charge-transfer energy parameter was varied from +9 eV to −5 eV corresponding to an almost linear variation in the ground state from $2p^63d^7$ to $2p^63d^8$. The multiplet features show up as multiple peaks that are more pronounced at the L_3 edge. For ΔE=−1 eV, one obtains a mixed ground state of equal weight of the $2p^63d^7$ and $2p^63d^8$ state, according to the number of unoc-

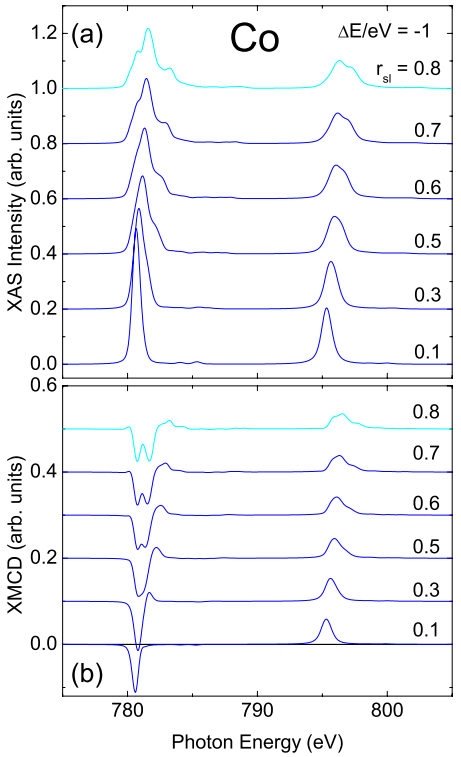

FIG. 7. (Color online) (a) Series of XAS charge-transfer multiplet calculations with varying reduction factor r_{sl} of the Slater integrals for the Co $2p^63d^7$ plus $2p^63d^8$ ground state at a charge-transfer energy of −1 eV (N_h=2.5). (b) Corresponding XMCD spectra.

cupied 3*d* holes of $N_h(Co)=2.5$ assumed for the sum-rule analysis.

Note that no resemblance with experimental Co XAS/XMCD spectra appears for any charge-transfer values. The extra peak at 1 eV above the L_3 XMCD maximum appearing for $\Delta E > -2$ eV and also visible in experiment is accompanied by a similar peak in the L_3 XAS spectra, which is not observed experimentally.

A reduction in the Slater integrals to 80% of the Hartree-Fock calculated values has been shown to be close to the optimized value to simulate the multiplet spectra of atoms.[24] For itinerant electron states of atoms in a metallic surrounding, one might expect an even larger reduction. Figure 7 shows the change in the spectra from the atomic multiplet features to the single peak at each *L* edge with decreasing core hole interaction. Thus, one may keep the one-electron model in cases where itinerant states sufficiently suppress this multiplet splitting of transition energies as, e.g., in intermetallic alloys and compounds.

Neglecting any multiplet effects, the simplest model of resonant x-ray absorption describes the photon absorption as an excitation of a core electron into unoccupied states[21] [see Fig. 8(b)]. The x-ray absorption of circularly polarized light may then be explained by a two-step process considering the dipole matrix elements. In the first step, the photoelectron is excited from a spin-orbit split $2p_{3/2}$ or $2p_{1/2}$ level ($L_{2,3}$ edge) and has taken up the angular momentum of the photon in part to its spin due to spin-orbit coupling.[21] Therefore, the

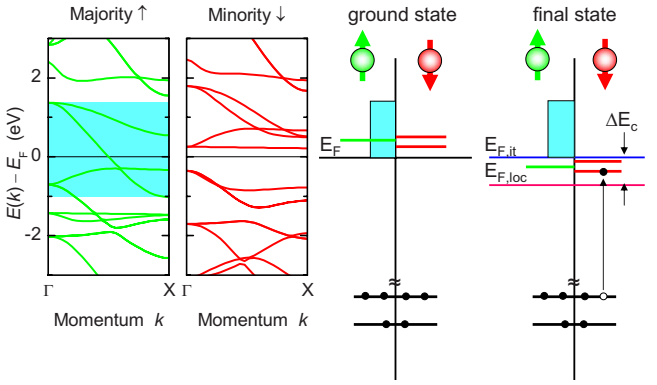

FIG. 8. (Color online) (Left) Calculated band structure for Co_2TiGe. (Right) Schematic description of the absorption process emphasizing the different reference energies for the localized and the delocalized 3*d* final-state configurations separated by ΔE_c.

excited photoelectrons might be considered spin polarized depending on the polarization direction of the incident light. Since the L_3 and L_2 edges have opposite spin-orbit coupling, the spin polarization is opposite at both edges. In a second step, the unoccupied valence-band states serve as a detector for the spin and orbital polarization. As the orbital magnetic moments in Heusler alloys are typically less then 10% of the spin moment, the orbital polarization of the photoelectrons can be neglected for the following discussion. For 2*p* to 3*d* transitions, the spin polarization is 25% at the L_3 edge and −50% at the L_2 edge. Transitions from 2*p* to 4*s* states are largely suppressed due to the small transition matrix element. Effects from anisotropic charge and spin densities may be neglected for the discussion of polycrystalline samples. Since the radial matrix elements show in general only a small energy dependence, the absorption spectra may be interpreted as a direct image of the spin-resolved PDOS above the Fermi energy. This simple interpretation of course requires that the angular matrix elements can be averaged at every energy value, i.e., 3*d* states of different magnetic quantum number equally contribute to the spectral density independent on energy. As has been shown for $Co_2(Fe_xMn_{1-x})Si$ and $Co_2Fe(Al_{0.5}Si_{0.5})$, this assumption holds to some extent in the case of the Co *L*-edge spectra.[30]

Within the constraints discussed above, the spin-resolved unoccupied PDOS $D^{\uparrow(\downarrow)}(1-f_F)$ (Fermi function f_F) follows from the XAS spectra μ^+ and μ^- according to

$$D^{\uparrow(\downarrow)}(1-f_F) \propto \mu_{iso} - s + (-)\frac{1}{P_j}\frac{\mu^+ - \mu^-}{2}, \qquad (1)$$

where μ_{iso} denotes the isotropic absorption coefficient $(\mu^+ + \mu^-)/2$, *s* is the step function and P_j is the spin polarization of the excited photoelectrons, i.e., $P_{L3}=0.25$ and $P_{L2}=-0.5$.

However, the Co states in Heusler alloys take an intermediate position between localized and delocalized states. Therefore, one has to consider core hole interaction at least to the lowest order. That means that the core hole in the final state attracts the excited electron, thus, lowering the energy needed for excitation when compared to the corresponding ground-state values. In principal, this energy rescaling occurs

for all x-ray absorption spectra. It is usually neglected, as it shifts the energy of the absorption energy by a constant value for all states. For Heusler alloys, however, the electronic states close to the Fermi energy are dominated by two different types of electronic states that can be classified as localized $3d-e_g$ and itinerant $3d-t_{2g}$ states. In the case of Co_2FeSi, the itinerant band dominates the unoccupied majority states near E_F,[10] while the minority states close to E_F are dominated by localized states. This is the case for most of the Co-based Heusler alloys. The core hole in the final state attracts the electron in the localized $3d$ states to a larger extent, thus, lowering the photon energy needed for the transition. For an itinerant state, the energy decrease is smaller since the electrons from neighboring atoms screen the core hole to some extent.[56,57] For a free-electron state, this final-state effect would completely vanish and the excitations energy equals the value following from the one-electron model. The different core hole screening thus produces an energy shift ΔE_c between itinerant and localized states [see also Fig. 8(b)].[56,57] A similar effect has been observed in V K-edge absorption spectra for VO_x (Ref. 57).

The exact value of ΔE_c is very critical for the determination of half-metallic properties from the XMCD data. ΔE_c is related to the bandwidth or, in other words, to the degree of localization of the contributing states. To the first order, it does not depend on the magnetic moment as given by the difference of unoccupied majority and minority states. For many Co-based Heusler compounds, calculations reveal a rather similar band structure close to E_F independent of the occupancy of the Y and Z sites except for a relative shift of each contributing band. Thus, one expects to first order a constant value of ΔE_c. In the case of Co_2TiSi ($N_v-24=2$), the majority electron states are composed of both itinerant and localized states at E_F. In this case, one expects a splitting of the onset of unoccupied majority states at E_F. The splitting allows for a direct experimental determination of $\Delta E_c=0.5$ eV as shown below. In the case of Co_2FeSi ($N_v-24=6$), a close comparison with *ab initio* calculation using a parameter-free LDA+DMFT ansatz[58] led to the same value. Moreover, the same calculation predicted a shift of E_F with respect to the conduction-band edge of minority electrons for the series $Co_2(Fe_xMn_{1-x})Si$ ($N_v-24=5-6$), which could be confirmed using a constant value of $\Delta E_c=0.5$ eV.[30] Therefore, we assume in the following this constant value for the determination of the position of E_F.

An analysis of Fe, Mn, Cr, and Ti spectra with respect to an evaluation of the PDOS is increasingly difficult because of the increasing localization and increasing contribution of multiplet effects as discussed in Ref. 24. For example, the Mn $L_{2,3}$ spectra in Co_2MnSi are convincingly explained by multiplet calculations based on atomic states (see Ref. 25). A combination of band-structure calculations and multiplet calculations will possibly enable a recovering of the Fe, Mn, Cr, or Ti PDOS from experimental data, but they are not available at present. However, an encouraging *ab initio* configuration-interaction method has recently been presented for the case of molecular orbitals.[59]

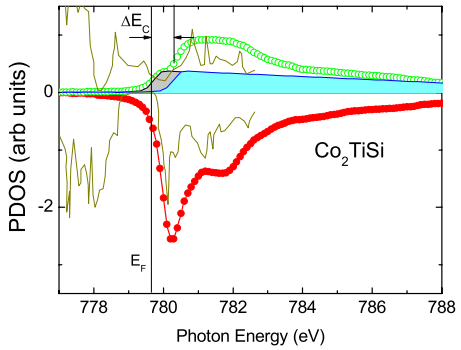

FIG. 9. (Color online) Spin-resolved PDOS calculated from the XAS/XMCD data measured at the L_3 edge. Majority PDOS (green circles) and minority PDOS (red bullets) are shown on a positive scale and negative scale, respectively. Full lines with shadings indicate the function used for approximation of the itinerant band as measured (blue) and shifted by ΔE_C (gray). Theoretical data from Ref. 31 are shown for comparison.

VII. SPIN-RESOLVED UNOCCUPIED DENSITY OF STATES

According to Eq. (1), we calculated the spin-resolved unoccupied PDOS function $D^{\uparrow(\downarrow)}$ for Co_2TiSi from data at the L_3 edge (see Fig. 9). For consideration of the thermal magnetization decrease at 300 K, we multiplied the XMCD signal by a factor $M(0)/M(T)=1.66$ for the cases of Co_2TiZ ($Z=$ Si, Ge, and Sn). The majority PDOS shows a characteristic double step increase at E_F, which can be directly related to the onset of the localized majority states at E_F and the onset of the itinerant majority state shifted by $\Delta E_C=0.5$ eV to higher energy. The experimental data fit well to the PDOS calculated in Refs. 29 and 31. The minority PDOS shows a sharp onset above E_F with an inclination point at $E_F+0.3$ eV, as expected for a half-metal. The broadening of the spectra caused by the finite lifetime of the excited state and by the limited energy resolution, however, hinders a direct determination of the spin polarization at E_F from this data. The same result can be calculated from the L_2 edge as discussed in Ref. 30. But $D^{\uparrow(\downarrow)}$ derived from the L_2 edges shows an even larger broadening because of the Coster-Kronig decay.[24]

In order to account for the lifetime broadening of the XAS/XMCD spectra, we have measured XAS data for Co_2MnSi with high resolution ($\Delta E=0.1$ eV) as shown in Fig. 10. We determined the Co PDOS according to Eq. (1) and deconvoluted the spectra with a Lorentzian function of various widths Γ. The results compared in Fig. 10 reveal an increasing steepness of the initial onset with increasing value of Γ. However, values larger than $\Gamma=0.4$ eV lead to an increasing contribution of oscillations, in particular, for $E<E_F$ indicating an overestimation of the lifetime broadening. The observation of a zero line for $E<E_F$ for $\Gamma=0.4$ eV is a consequence of a near coincidence of the Lorentzian function and the experimental data. Note that for $\Gamma=0.4$ eV, the Co minority PDOS is close to zero in a finite-energy interval around E_F. Thus, the experimental data support the theoretical prediction of Co_2MnSi being a half-metal even if ΔE_C slightly differs from the assumed value. Attempts of using a

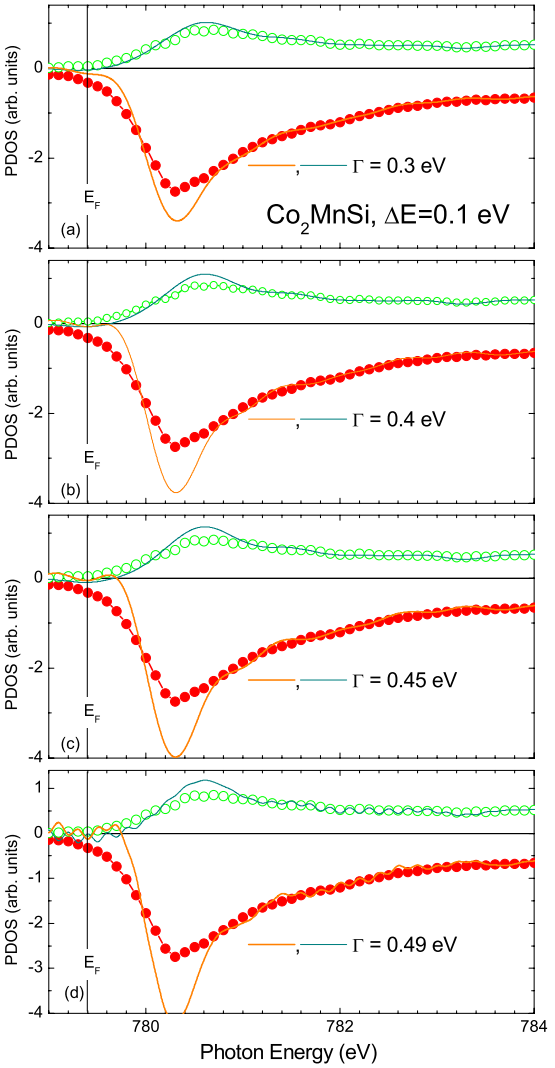

FIG. 10. (Color online) Spin-resolved PDOS calculated from the XAS/XMCD data measured at the L_3 edge of a Co_2MnSi film with similar spectra as the bulk data. Majority PDOS (green circles) and minority PDOS (red bullets) are shown on a positive scale and negative scale, respectively. Data after deconvolution with a Lorentzian function (full lines) of width Γ as indicated in the figure.

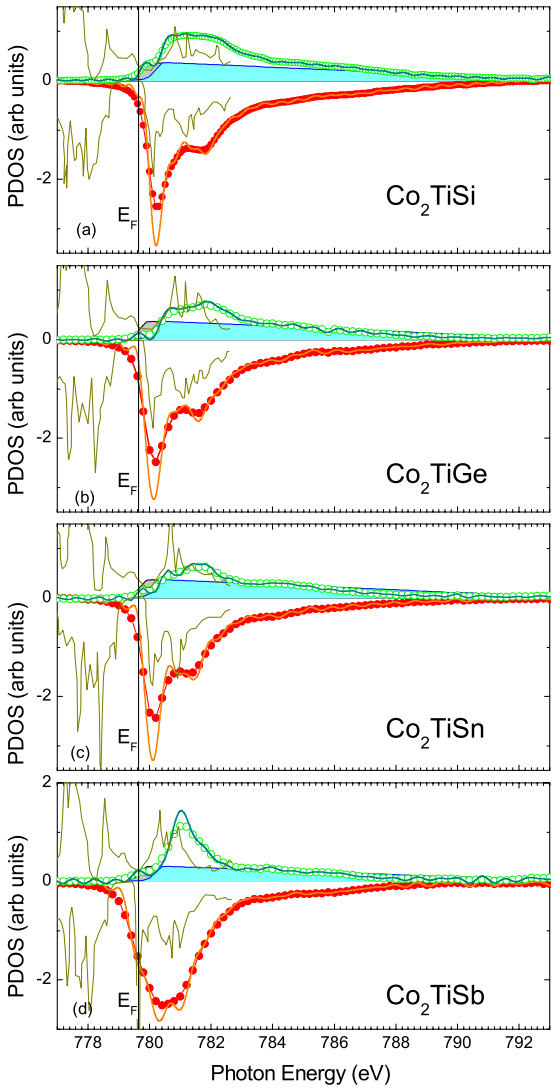

FIG. 11. (Color online) Spin-resolved PDOS calculated from the XAS/XMCD data measured at the L_3 edge for samples as indicated in the figure. Full lines indicate deconvoluted data. Full lines with shadings indicate the function used for approximation of the itinerant band as measured (blue) and shifted by ΔE_C (gray). Theoretical data from Ref. 31 are shown for comparison.

deconvolution function of a convoluted Lorentzian and Gaussian function in order to consider the finite-energy resolution led to an increased contribution of oscillations and were therefore abandoned. In the following, we have applied a Lorentzian function with a constant value of $\Gamma = 0.4$ eV for deconvolution of the experimental data.

Figure 11 shows the Co PDOS for the sample series Co_2TiZ ($Z=$ Si, Ge, Sn, and Sb) recovered from the L_3 edge data including a scaling factor $M(0)/M(T)$ for the case of $Z=$ Si, Ge, and Sn. The Co PDOS for $Z=$ Si, Ge, and Sn look similar to each other which can be expected because the compounds are isoelectronic to each other.[31] For all samples, the majority PDOS shows a characteristic double step increase at E_F although the steps are less pronounced for the cases of $Z=$ Ge, Sn, and Sb compared to $Z=$ Si. The double step indicates the simultaneous presence of itinerant and localized majority states at E_F. We assume in the following that the contribution of the itinerant band is constant for all Co-based Heusler compounds. This assumption is supported by the fact that calculations reveal a similar width of the itinerant band (approximately 4 eV) for all these compounds. The contribution from the itinerant band is approximated by a steplike function with slowly decreasing intensity for increasing energy. We have used the same function for all samples. We shifted the function along the energy axis in order to fit the onset of the itinerant contribution to the majority bands. Then we subtracted from the 50% point of the step function the correlation energy $\Delta E_C = 0.5$ eV in order to determine E_F corresponding to the localized majority and minority contributions to the PDOS.

The minority PDOS shows a pronounced maximum at $E_{v,max} - E_F = 0.5$ eV. The maximum is related to the unoccupied Co e_g state.[31] The binding energy of this state is in accordance with most calculations.[29,31] In contrast, Ref. 60

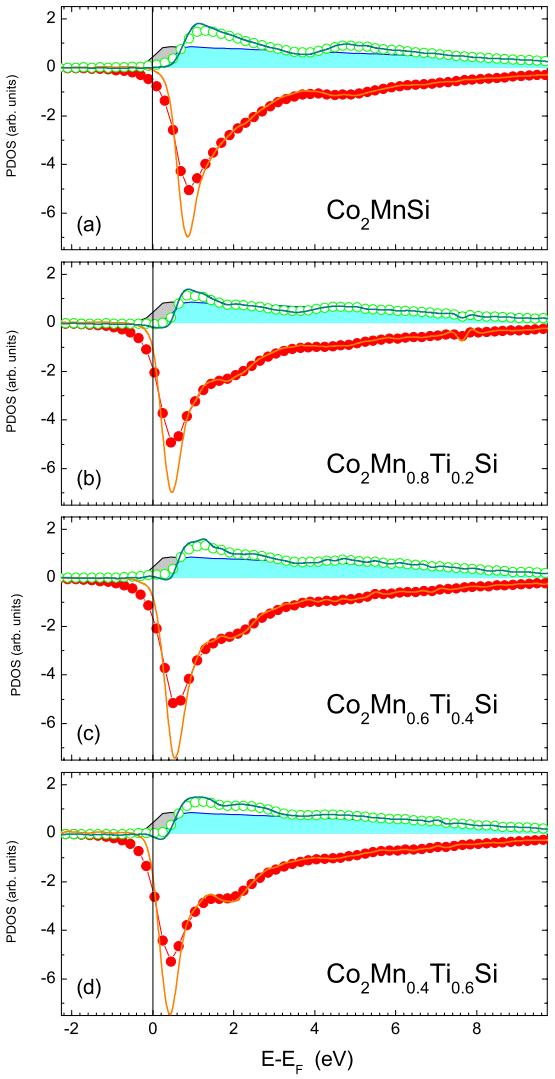

FIG. 12. (Color online) Spin-resolved PDOS calculated from the XAS/XMCD data measured at the L_3 edge for samples as indicated in the figure. Same notation as in Fig. 11.

predicts much larger values ($E_{v,max}-E_F=1-2$ eV) for Co_2TiSn depending on the calculation scheme. From comparison with theory, we can identify the second maximum of the minority PDOS at $E-E_F=2$ eV as a localized Co-Ti hybridization state of t_{2g} character. It is this pronounced t_{2g} hybridization peak that causes the double peak feature in the Co XAS spectrum (Fig. 1). Upon approaching E_F, the minority PDOS rapidly decreases but does not vanish at E_F. Therefore, Co_2TiZ with $Z=$ Si, Ge, and Sn are at the boundary of being half-metallic with E_F positioned at the minority conduction-band edge.

For Co_2TiSb, the minority PDOS does not decrease close to E_F but instead reveals a shoulder directly at E_F. This reflects the metallic behavior of this particular compound in agreement with a calculation by Lee *et al.*[31]

For the $Co_2(Mn_xTi_{1-x})Si$ series shown in Fig. 12, the minority feature caused by the Co-Ti t_{2g} state gradually decreases with decreasing Ti concentration. For Co_2MnSi, the corresponding Co-Mn t_{2g} state produces a much weaker feature at a slightly larger energy in accordance with calculations.[28] We do not observe a gradual shift of the minority maximum with the change in composition. Instead, $E_{v,max}$ remains at 0.5 eV above E_F with increasing Mn concentration for $x\leq 0.8$ and increases to 0.9 eV for $x=1$.

The Co PDOS of Co_2MnGe [Fig. 13(a)] appears similar to the corresponding spectra for Co_2MnSi as expected from theory.[28] Close inspection reveals a little more pronounced Co-Mn t_{2g} feature at $E-E_F=2.3$ eV in accordance with Ref. 28. The most prominent difference, however, is the reduced energy of the minority maximum at $E_{v,max}-E_F=0.7$ eV compared to $E_{v,max}-E_F=0.9$ eV for Co_2MnSi. Calculations using the same approximations for Co_2MnSi and Co_2MnGe predicted the same energy of 0.7 eV for both compounds.[28] For Co_2MnGa, the minority maximum is located at a larger energy $E_{v,max}-E_F=1.0$ eV in excellent agreement with Ref. 28. The Co-Mn t_{2g} feature is weaker and the Co-Ga hybridization state appears at 5.5 eV instead of 4.5 eV for Co_2MnGe. For the $Co_2Mn(Ga_{1-x}Ge_x)$ series, we observe a gradual shift of the minority maximum from 0.7 to 1.0 eV with increasing Ga concentration. The rapid decrease in the minority maximum close to E_F is compatible with the predicted half-metallic properties for the whole series. The gradual shift demonstrates the proposed concept of varying the position of E_F relative to the minority band gap.

Figure 14 summarizes results for the separation of the minority PDOS maximum and the Fermi energy $E_{v,max}-E_F$. For the $Co_2(Mn_xTi_{1-x})Si$ series, the spin-resolved Co PDOS reveals a minority maximum at a constant value $E_{v,max}-E_F=0.5$ eV for $x<1$ and a rapid increase to 0.9 eV for $x=1$. This behavior is in contrast to the gradual shift expected from the rigid-band model. Instead, we observe a linear shift of $E_{v,max}-E_F$ for the series $Co_2Mn(Ga_{1-x}Ge_x)$ with increasing x. *Ab initio* calculations have predicted this trend for the analogous main group substitution series $Co_2Fe(Al_{1-x}Si_x)$ (Ref. 15).

VIII. CONCLUSIONS

Magnetic properties and electronic structures of Co_2TiZ ($Z=$ Si, Ge, Sn, and Sb) and the substitutional series $Co_2(Mn_xTi_{1-x})Si$ and $Co_2Mn(Ga_{1-x}Ge_x)$ were investigated by XAS and XMCD. Applying the sum-rule analysis, we determined element-specific magnetic moments for Co, Mn, and Ti. The Ti moment is in all samples rather small ($<0.03\mu_B$) and oriented antiparallel to the mean magnetization direction, indicating that Ti containing Heusler compounds are ferrimagnets. The Mn moments are comparatively large ($>3\mu_B$), consisting mainly of a spin moment as the orbital to spin ratio is less than 0.03. The Co moment shows values of $0.8-1.0\mu_B$, extrapolated to 0 K in the case of Co_2TiZ. Co_2TiSb is an exception with a vanishing Ti moment and a smaller Co moment.

For the parent compounds with $x=0$ and $x=1$, the total magnetization and the element-specific moments are in agreement with previously reported theoretical and experimental results. The substitutional series of quaternary Heusler compounds proposed for a tuning of the band structure are expected to show a linearly increasing magnetization with increasing number of valence electrons, i.e., propor-

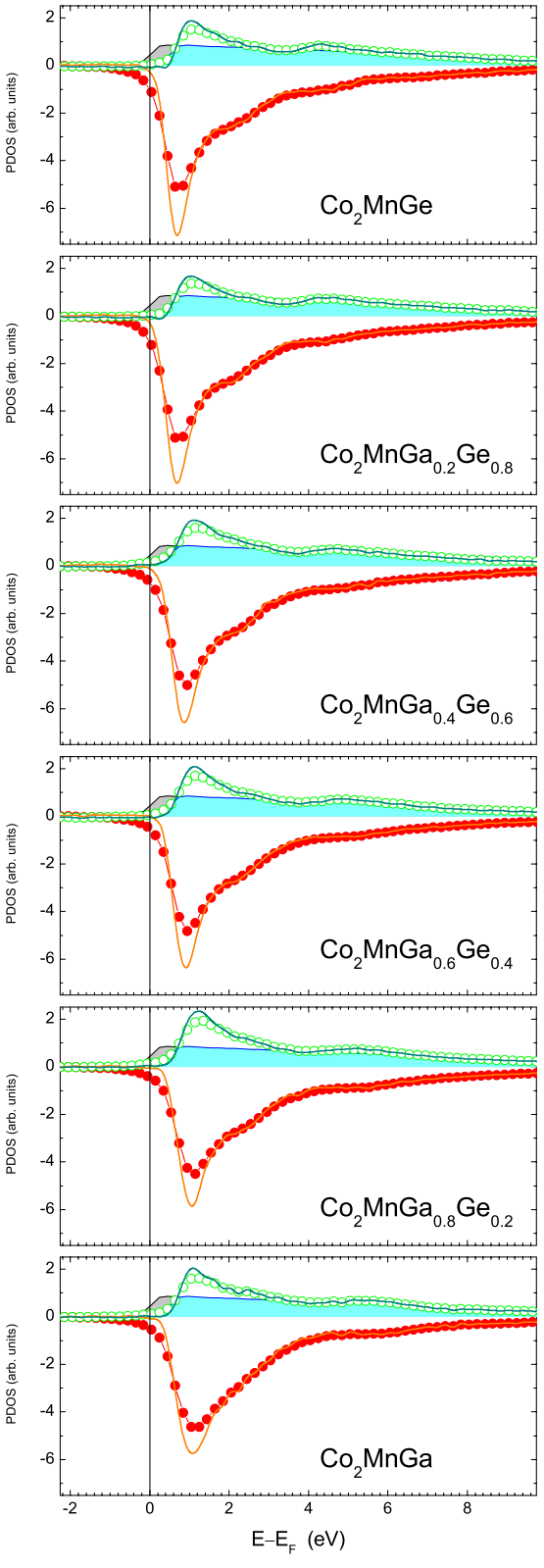

FIG. 13. (Color online) Spin-resolved PDOS calculated from the XAS/XMCD data measured at the L_3 edge for samples as indicated in the figure. Same notation as in Fig. 11.

tional to N_v-24, thus, obeying the generalized Slater-Pauling rule. For the $Co_2(Mn_xTi_{1-x})Si$ series, we observed a magnetization slightly exceeding values according to the Slater-Pauling rule. Similar observations were reported in the case of the substitutional series $Co_2Mn_{1-x}Fe_xAl$ (Ref. 49) and attributed to partial disorder. For the $Co_2Mn(Ga_{1-x}Ge_x)$ series, we measured magnetization values in agreement with the Slater-Pauling rule.

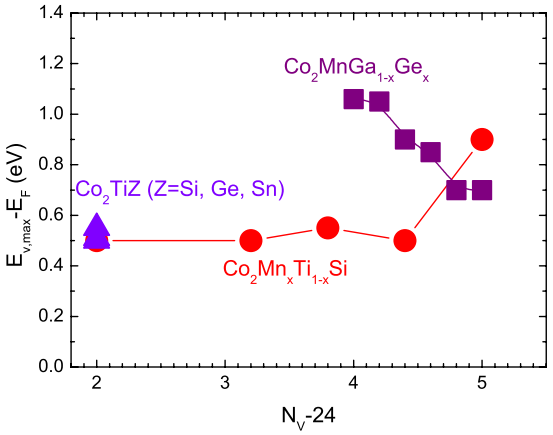

FIG. 14. (Color online) Separation of the minority PDOS maximum and the Fermi energy $E_{v,max}-E_F$ for the indicated Heusler alloys (full symbols). N_v indicates the number of valence electrons per formula unit.

Two complementary series are investigated with transition-metal substitution on the Y site and main group element substitution on the Z site. We find that the distribution of the magnetization on the X and Y sublattices varies with N_v in a similar way for the two complementary series. For $Co_2(Mn_xTi_{1-x})Si$, the element-specific moments remain almost constant and the increase in the magnetization with increasing x is directly related to the increasing Mn content. Thus, the Y sublattice covers the total magnetization increase. For $Co_2Mn(Ga_{1-x}Ge_x)$, we find an almost constant Co moment and an increasing Mn moment on the Y sublattice. The almost constant Co moment reflects the fact that the distribution of the Co d electrons in the majority and minority states does not change with N_v.[29] In order to maximize the number of unpaired electrons, the minority d states should be filled by eight electrons to have a gap and the rest of the electrons fill the majority states.[61] As the Co minority d states are occupied by roughly 3.5 electrons at each atom, only one minority d electron stems from the Y atom. This explains the increasing moment on the Y site going from Ti to Mn. The increase in the Mn moment for $Co_2Mn(Ga_{1-x}Ge_x)$ cannot be explained by this general behavior of d electrons. In this case, the hybridization of electrons at the Z site causes a redistribution of majority and minority electrons when the Ga is replaced by Ge. Because Ge has a higher electronegativity compared to Ga, the bonding interaction between Co and Ge is stronger than for Co and Ga. This causes an electron transfer to delocalized states in the interstitial. In particular, the t_{2g} minority states at the Y site are emptied. At the same time, the majority t_{2g} states are filled resulting in a larger moment.

Although the orbital moment contributes less than 10% to the total moment, its variation with composition is an important indication for local deviations from cubic symmetry. Large orbital moments may also be a hint to an increased

magnetic crystal anisotropy and to an increased Gilbert damping.[62,63] We find orbital magnetic moments to be low for the parent Heusler compounds and increased values in the case of mixed compounds, i.e., $0<x<1$. For $Co_2(Mn_xTi_{1-x})Si$, the maximum orbital moment appears at $x=0.8$ and for $Co_2Mn(Ga_{1-x}Ge_x)$ at $x=0.6$. We attribute this observation to a local distortion from the cubic symmetry caused by a random occupation of the *Y* and *Z* sites, respectively.

Considering final-state electron correlation, the spin-resolved PDOS at the Co atom can be extracted from the XMCD data. As the minority Co states are closest to the Fermi edge, the partial density of Co states is decisive for the half-metallic properties of the Co-based Heusler compounds. The experimental results confirm theoretical predictions for the PDOS in the case of Co_2TiSi, Co_2TiGe, and Co_2TiSn. The Fermi energy E_F is located at the minority conduction-band edge. This means that these compounds are at the borderline of being half-metallic. In contrast, Co_2TiSb shows a large minority PDOS at the Fermi energy like a normal metal.

The idea of tailoring the electronic structure in substitutional quaternary Heusler compounds originates from the rigid-band model. Accordingly, an increasing number of valence electrons fill previously unoccupied states, thus, lifting the Fermi energy with respect to the rigid-band structure. Consequently, one expects that $E_{v,max}-E_F$ decreases with increasing N_v. This is indeed observed for $Co_2Mn(Ga_{1-x}Ge_x)$ and also for $Co_2Mn_{1-x}Fe_xSi$.[30] For the series $Co_2MnGa_{1-x}Ge_x$, we observe a gradual shift of the minority PDOS maximum from 0.7 eV for $x=1$ to 1.0 eV for $x=0$ and also a gradual increase in the onset of the minority PDOS with decreasing *x*. Thus, the Co minority PDOS corroborates half-metallic ferromagnetism for the whole series.

In contrast, $E_{v,max}-E_F$ increases with increasing N_v for $Co_2(Mn_xTi_{1-x})Si$, indicating a reversed electron transfer out of the Co *d* majority states. Note that due to the small density of Co states at the Fermi edge, a small charge transfer that is negligible for the magnetic moment causes a sizable shift. A second deviation from the rigid-band model is revealed by the comparison of Co_2MnSi and Co_2MnGe. Although N_v is not changed, we observe different values for $E_{v,max}-E_F$.

Ab initio calculations, explaining qualitatively the trends in the case of $Co_2(Mn_xTi_{1-x})Si$ and $Co_2Mn(Ga_{1-x}Ge_x)$, show quantitative deviations from our results and with each other depending on the model assumptions. In addition, an exchange of the main group element with an element from the same group should have a negligible influence on the band structure according to theory. The deviation from that rule observed here for $Co_2(Mn_xTi_{1-x})Si$ and $Co_2Mn(Ga_{1-x}Ge_x)$ may be a hint to previously neglected electron correlation effects.

In summary, our results confirm the predicted possibility of tailoring the minority band gap using substitutional quaternary Heusler compounds. A detailed analysis reveals in some cases deviations from general assumptions related to a rigid-band model and also from standard *ab initio* calculations using local-density approximation, which are attributed to electron correlation effects.

ACKNOWLEDGMENTS

The authors are thankful for financial support from the DFG (Grant No. FOR 559) and the BMBF (Grant No. ES3XBA/5) and S. Cramm for support at BESSY.

*elmers@uni-mainz.de

[1] R. A. de Groot, F. M. Mueller, P. G. vanEngen, and K. H. J. Buschow, Phys. Rev. Lett. **50**, 2024 (1983).
[2] J. H. Park, E. Vescovo, H. J. Kim, C. Kwon, R. Ramesh, and T. Venkatesan, Nature (London) **392**, 794 (1998).
[3] K. Inomata, S. Okamura, R. Goto, and N. Tezuka, Jpn. J. Appl. Phys. **42**, L419 (2003).
[4] S. Kammerer, A. Thomas, A. Hütten, and G. Reiss, Appl. Phys. Lett. **85**, 79 (2004).
[5] Y. Sakuraba, M. Hattori, M. Oogane, Y. Ando, H. Kato, A. Sakuma, T. Miyazaki, and H. Kubota, Appl. Phys. Lett. **88**, 192508 (2006).
[6] W. Wang, H. Sukegawa, R. Shan, and K. Inomata, Appl. Phys. Lett. **93**, 122506 (2008).
[7] S. Tsunegi, Y. Sakuraba, M. Oogane, K. Takanashi, and Y. Ando, Appl. Phys. Lett. **93**, 112506 (2008).
[8] I. Galanakis, P. H. Dederichs, and N. Papanikolaou, Phys. Rev. B **66**, 174429 (2002).
[9] S. Picozzi, A. Continenza, and A. J. Freeman, Phys. Rev. B **66**, 094421 (2002).
[10] C. Felser, G. Fecher, and B. Balke, Angew. Chem., Int. Ed. **46**, 668 (2007).
[11] N. Tezuka, N. Ikeda, S. Sugimoto, and K. Inomata, Jpn. J. Appl. Phys., Part 2 **46**, L454 (2007).
[12] L. Chioncel, Y. Sakuraba, E. Arrigoni, M. I. Katsnelson, M. Oogane, Y. Ando, T. Miyazaki, E. Burzo, and A. I. Lichtenstein, Phys. Rev. Lett. **100**, 086402 (2008).
[13] G. H. Fecher, H. C. Kandpal, S. Wurmehl, J. Morais, H. Lin, H. J. Elmers, G. Schönhense, and C. Felser, J. Phys.: Condens. Matter **17**, 7237 (2005).
[14] K. Özdogan, B. Aktas, I. Galanakis, and E. Sasioglu, J. Appl. Phys. **101**, 073910 (2007).
[15] G. H. Fecher and C. Felser, J. Phys. D **40**, 1582 (2007).
[16] Z. Gercsi and K. Hono, J. Phys.: Condens. Matter **19**, 326216 (2007).
[17] R. Shan, H. Sukegawa, W. H. Wang, M. Kodzuka, T. Furubayashi, T. Ohkubo, S. Mitani, K. Inomata, and K. Hono, Phys. Rev. Lett. **102**, 246601 (2009).
[18] B. Balke, G. H. Fecher, H. C. Kandpal, C. Felser, K. Kobayashi, E. Ikenaga, J. J. Kim, and S. Ueda, Phys. Rev. B **74**, 104405 (2006).
[19] G. H. Fecher, B. Balke, S. Ouardi, C. Felser, G. Schonhense, E. Ikenaga, J. Kim, S. Ueda, and K. Kobayashi, J. Phys. D **40**, 1576 (2007).
[20] J. Schmalhorst, D. Ebke, A. Weddemann, A. Hütten, A. Thomas, G. Reiss, A. Turchanin, A. Gölzhäuser, B. Balke, and C. Felser,

J. Appl. Phys. **104**, 043918 (2008).
[21] J. Stöhr, J. Magn. Magn. Mater. **200**, 470 (1999).
[22] H. Ebert, Rep. Prog. Phys. **59**, 1665 (1996).
[23] V. N. Antonov, D. A. Kukusta, A. P. Shpak, and A. N. Yaresko, Condens. Matter Phys. **11**, 627 (2008).
[24] F. M. F. de Groot, J. C. Fuggle, B. T. Thole, and G. A. Sawatzky, Phys. Rev. B **42**, 5459 (1990).
[25] N. D. Telling, P. S. Keatley, G. van der Laan, R. J. Hicken, E. Arenholz, Y. Sakuraba, M. Oogane, Y. Ando, K. Takanashi, A. Sakuma, and T. Miyazaki, Phys. Rev. B **78**, 184438 (2008).
[26] G. Jakob, T. Eichhorn, M. Kallmayer, and H. J. Elmers, Phys. Rev. B **76**, 174407 (2007).
[27] M. Kallmayer, K. Hild, T. Eichhorn, H. Schneider, G. Jakob, A. Conca, M. Jourdan, H. J. Elmers, A. Gloskovskii, S. Schuppler, and P. Nagel, Appl. Phys. Lett. **91**, 192501 (2007).
[28] I. Galanakis, Ph. Mavropoulos, and P. H. Dederichs, J. Phys. D **39**, 765 (2006).
[29] H. C. Kandpal, G. H. Fecher, and C. Felser, J. Phys. D **40**, 1507 (2007).
[30] M. Kallmayer, P. Klaer, H. Schneider, E. Arbelo Jorge, C. Herbort, G. Jakob, M. Jourdan, and H. J. Elmers, Phys. Rev. B **80**, 020406(R) (2009).
[31] S. C. Lee, T. D. Lee, P. Blaha, and K. Schwarz, J. Appl. Phys. **97**, 10C307 (2005).
[32] H. C. Kandpal, V. Ksenofontov, M. Wojcik, R. Seshadri, and C. Felser, J. Phys. D **40**, 1587 (2007).
[33] J. Barth, G. Fecher, B. Balke, T. Graf, C. Felser, A. Shkabko, and A. Weidenkaff, arXiv:0907.3562 (unpublished).
[34] B. Balke, G. H. Fecher, and C. Felser, Appl. Phys. Lett. **90**, 242503 (2007).
[35] K. Miyamoto, A. Kimura, K. Iori, T. Xie, K. Sakamoto, T. Moko, S. Qiao, M. Taniguchi, and K. Tsuchiyac, Physica B **351**, 347 (2004).
[36] M. Kallmayer, H. Schneider, G. Jakob, H. J. Elmers, K. Kroth, H. Kandpal, U. Stumm, and C. Cramm, Appl. Phys. Lett. **88**, 072506 (2006).
[37] T. Graf, F. Casper, J. Winterlik, B. Balke, G. H. Fecher, and C. Felser, Z. Anorg. Allg. Chem. **635**, 976 (2009).
[38] H. J. Elmers, G. H. Fecher, D. Valdaitsev, S. A. Nepijko, A. Gloskovskii, G. Jakob, G. Schönhense, S. Wurmehl, T. Block, C. Felser, P.-C. Hsu, W.-L. Tsai, and S. Cramm, Phys. Rev. B **67**, 104412 (2003).
[39] A. Scherz, H. Wende, and K. Baberschke, Appl. Phys. A: Mater. Sci. Process. **78**, 843 (2004).
[40] C. T. Chen, Y. U. Idzerda, H.-J. Lin, N. V. Smith, G. Meigs, E. Chaban, G. H. Ho, E. Pellegrin, and F. Sette, Phys. Rev. Lett. **75**, 152 (1995).
[41] R. Nakajima, J. Stöhr, and Y. U. Idzerda, Phys. Rev. B **59**, 6421 (1999).
[42] A. Yamasaki, S. Imada, R. Arai, H. Utsunomiya, S. Suga, T. Muro, Y. Saitoh, T. Kanomata, and S. Ishida, Phys. Rev. B **65**, 104410 (2002).
[43] L. V. Bekenov, V. N. Antonov, A. P. Shpak, and A. N. Yaresko, Condens. Matter Phys. **8**, 565 (2005).
[44] J. Schmalhorst, S. Kämmerer, M. Sacher, G. Reiss, A. Hütten, and A. Scholl, Phys. Rev. B **70**, 024426 (2004).
[45] M. Kallmayer, H. J. Elmers, B. Balke, S. Wurmehl, F. Emmerling, G. H. Fecher, and C. Felser, J. Phys. D **39**, 786 (2006).
[46] J. Grabis, A. Bergmann, A. Nefedov, K. Westerholt, and H. Zabel, Phys. Rev. B **72**, 024437 (2005).
[47] P. Klaer, M. Kallmayer, H. J. Elmers, L. Basit, J. Thoene, S. Chadov, and C. Felser, J. Phys. D **42**, 084001 (2009).
[48] K. Miyamoto, K. Iori, A. Kimura, T. Xie, M. Taniguchi, S. Qiao, and K. Tsuchiya, Solid State Commun. **128**, 163 (2003).
[49] V. Jung, G. H. Fecher, B. Balke, V. Ksenofontov, and C. Felser, J. Phys. D **42**, 084007 (2009).
[50] J. H. Kohlhepp, H. Swagten, C. Blum, and C. Felser (unpublished).
[51] M. Sargolzaei, M. Richter, K. Koepernik, I. Opahle, H. Eschrig, and I. Chaplygin, Phys. Rev. B **74**, 224410 (2006).
[52] P. Gambardella, S. S. Dhesi, S. Gardonio, C. Grazioli, P. Ohresser, and C. Carbone, Phys. Rev. Lett. **88**, 047202 (2002).
[53] K. W. Edmonds, N. R. S. Farley, T. K. Johal, G. van der Laan, R. P. Campion, B. L. Gallagher, and C. T. Foxon, Phys. Rev. B **71**, 064418 (2005).
[54] R. D. Cowan, *The Theory of Atomic Structure and Spectra* (University of California Press, Berkeley, 1981).
[55] The calculations have been performed with the program MISSING 1.1 by Riccardo Gusmeroli and Claudia Dallera and with the program CTM4XAS by Eli Stavitski and Frank de Groot. Both codes are based on Cowan's Hartree-Fock atomic code.
[56] P. J. W. Weijs, M. T. Czyzyk, J. F. van Acker, W. Speier, J. B. Goedkoop, H. van Leuken, H. J. M. Hendrix, R. A. de Groot, G. van der Laan, K. H. J. Buschow, G. Wiech, and J. C. Fuggle, Phys. Rev. B **41**, 11899 (1990).
[57] A. Bianconi, Phys. Rev. B **26**, 2741 (1982).
[58] S. Chadov, G. H. Fecher, C. Felser, J. Minar, J. Braun, and H. Ebert, J. Phys. D **42**, 084002 (2009).
[59] H. Ikeno, F. M. F. de Groot, E. Stavitski, and I. Tanaka, J. Phys.: Condens. Matter **21**, 104208 (2009).
[60] M. C. Hickey, A. Husmann, S. N. Holmes, and G. A. C. Jones, J. Phys.: Condens. Matter **18**, 2897 (2006).
[61] J. Kübler, Physica B **127**, 257 (1984).
[62] T. Kubota, S. Tsunegi, M. Oogane, S. Mizukami, T. Miyazaki, H. Naganuma, and Y. Ando, Appl. Phys. Lett. **94**, 122504 (2009).
[63] C. Liu, C. K. A. Mewes, M. Chshiev, T. Mewes, and W. H. Butler, Appl. Phys. Lett. **95**, 022509 (2009).